Analytica Chimica Acta xxx (2018) 1–8

Contents lists available at ScienceDirect

Analytica Chimica Acta

journal homepage: www.elsevier.com/locate/aca

Near-infrared MnCuInS/ZnS@BSA and urchin-like Au nanoparticle as a novel donor-acceptor pair for enhanced FRET biosensing

Hong Xing [a], Tianxiang Wei [b, *], Xin Lin [b], Zhihui Dai [a, c, **]

[a] Jiangsu Key Laboratory of Biofunctional Materials, School of Chemistry and Materials Science, Nanjing Normal University, Nanjing, 210023, PR China
[b] School of Environment, Nanjing Normal University, Nanjing, 210023, PR China
[c] Nanjing Normal University Center for Analysis and Testing, Nanjing, 210023, PR China

HIGHLIGHTS

- MnCuInS/ZnS QDs were encapsulated in BSA nanoparticles to improve the water solubility and amplify the fluorescent signal.
- The novel structure endows the Au NPs with strong surface plasma absorption to match with the NIR emission spectra.
- The NIR MnCuInS/ZnS@BSA and urchin-like Au NPs were first applied as a donor-acceptor pair for enhanced FRET biosensing.

GRAPHICAL ABSTRACT

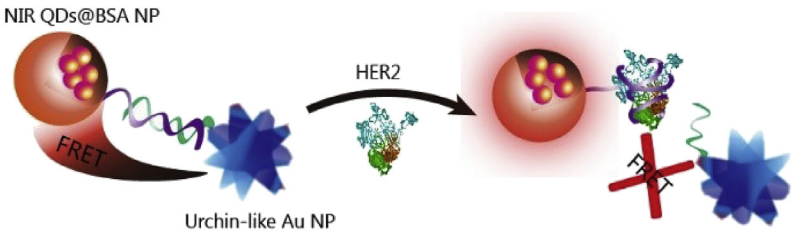

ARTICLE INFO

Article history:
Received 10 March 2018
Received in revised form
20 April 2018
Accepted 18 May 2018
Available online xxx

Keywords:
Near-infrared quantum dots
Urchin-like Au NPs
FRET
HER2 protein
Biosensor

ABSTRACT

An enhanced near-infrared (NIR) FRET biosensing system based on the novel donor-acceptor pair (MnCuInS/ZnS@BSA and urchin-like Au NPs) was developed for the sensitive detection of HER2 protein. In this strategy, MnCuInS/ZnS quantum dots (QDs) were chosen due to their NIR emission, high quantum efficiency, and low toxicity. Amounts of MnCuInS/ZnS QDs were encapsulated in BSA to form MnCuInS/ZnS@BSA nanoparticles, which can easily transfer MnCuInS/ZnS QDs from organic phase into aqueous solution, and the formed nanoparticles were applied as the energy donor which significantly enhanced the fluorescence intensity. As for the energy acceptor, urchin-like Au nanoparticles (Au NPs) with novel structure, good stability and excellent quenching ability towards NIR fluorescence were selected. Thus, the NIR MnCuInS/ZnS@BSA and urchin-like Au NPs were designed as a novel donor-acceptor pair for FRET assay. By combining the optical advantages of NIR QDs encapsulated BSA nanoparticles with the excellent fluorescence quenching ability of urchin-like Au NPs, the proposed FRET-based biosensor realized enhanced FRET effect for highly sensitive detection of HER2 in human serum samples. A wide detection range (2−100 ng mL^{-1}) and a low detection limit (1 ng mL^{-1}) were obtained. This sensing system can decrease the interference of other biomolecules in NIR region, can be applied to other biomarker determination in vitro, and also shows great potential for in vivo diagnosis.

* Corresponding author. School of Environment, Nanjing Normal University, Nanjing, 210023, PR China.
** Corresponding author. Jiangsu Key Laboratory of Biofunctional Materials, School of Chemistry and Materials Science, Nanjing Normal University, Nanjing, 210023, PR China.
E-mail addresses: weitian_xiang@126.com (T. Wei), daizhihuii@njnu.edu.cn (Z. Dai).

https://doi.org/10.1016/j.aca.2018.05.048
0003-2670/

1. Introduction

Nowadays, the technique of Fluorescence Resonance Energy Transfer (FRET) has attracted great attention in nucleic acid biosensing, cell imaging, immunoassays and other fields due to its unique advantages for homogeneous detection, including its non-invasion, convenience, simplicity, and high sensitivity [1–3]. The two major components in FRET technique are energy donors and acceptors. This requires seeking materials with good photoluminescence signal for energy donors and corresponding materials with absorbance within the range of energy donors' emission wavelength for energy acceptors [4–7]. Among the many materials used in FRET-based analysis, quantum dots (QDs) as a class of inorganic materials have been verified to be the efficient and promising energy donors owing to their prominent optical properties [8,9]. Compared with conventional energy donors-organic dyes, QDs have a number of unique characteristics, such as size and component-tunable narrow emission, outstanding resistance against photobleaching, long fluorescence lifetime and high fluorescence efficiency [10–13]. Their unique characteristics can enhance the FRET effect, thereby realizing the wide application in biological assays.

In recent years, biosensing in near infrared (NIR) region has gotten great attention [14,15] due to its reduced photo-damage, low background interference, and weak scattered light [1,16,17]. Recently, most of the QDs-based FRET biosensing were in visible region. To develop preferable QDs-based FRET systems in NIR region still remains a big challenge. The key point is to find out the proven and effective NIR donor-acceptor pair.

As we know, Au nanoparticles (Au NPs) are usually considered to be the star acceptors in FRET system due to their good stability, unfluctuating signal intensity, and strong resistance to photobleaching [18–20]. However, ordinary spherical Au NPs usually do not absorb the NIR region light. Fortunately, except for ordinary spherical Au nanomaterials, different shapes of Au nanomaterials with different absorption spectra have also been studied, such as nanorod, nanocube, nanobipyramid, nanoplate and various branched NPs. In our strategy, urchin-like Au NPs, a novel Au nanostructure, were selected as the energy acceptors. These ink blue urchin-like Au NPs have advantages of abundant nanobridges, large specific surface area, improved uniformity and strong surface plasma absorption in NIR region. Based on their strong absorption in NIR region, fluorescence quenching efficiency can be enhanced and the signal sensitivity can be improved [21]. Their diameters are tunable and their peaks of surface plasmon resonance absorption can be adjusted to match exactly with the emission spectra of NIR QDs.

As for the donors, a number of NIR QDs, such as CdTe/CdS [22], PbS [23], CdHgTe [24], and CdSeTe/ZnS [25], have been successfully used in cell imaging [26] and biomarker detection [27]. However, due to the presence of heavy metal elements, the high toxicity of these NIR QDs restricts their wide application in biology. Therefore, the development of heavy metal-free NIR QDs has become an emerging trend. With this in mind, doped QDs like MnCuInS QDs seem to be extremely promising candidates because they do not possess any toxic Class A elements (Cd, Hg, and Pb) or Class B elements (As and Se) [28,29]. Moreover, a ZnS shell can be introduced around the MnCuInS core nanocrystals to improve the photoluminescence quantum yields of MnCuInS [30,31].

MnCuInS/ZnS nanocrystals are usually synthesized in the organic phase, which shows limitation in biological applications. To make MnCuInS/ZnS QDs and urchin-like Au NPs into the proven and effective NIR donor-acceptor pair which can be used in FRET biosensing, the transfer of MnCuInS/ZnS QDs from organic phase to aqueous phase by surface modification is essential. Two kinds of basic methods have been developed. The first method is to replace the surface hydrophobic ligands on QDs with water-soluble stabilizers (i.e., the ligand exchange strategy). The second method is to encapsulate hydrophobic QDs with amphiphilic biomolecules (i.e., the encapsulation strategy) [32]. Compared with the water-soluble QDs obtained by the ligand exchange strategy, the colloidal stability of QDs obtained by the encapsulation strategy is generally higher under biological conditions [33].

In this work, the commercially available and cheap bovine serum albumin (BSA) was chosen to encapsulate amounts of MnCuInS/ZnS QDs to form MnCuInS/ZnS QDs encapsulated BSA nanoparticles. These MnCuInS/ZnS@BSA nanoparticles enabled long-term colloidal stability in aqueous media and significant enhanced fluorescence intensity. In addition, the abundant amino groups and carboxylate groups at the surface of MnCuInS/ZnS@BSA nanoparticles allowed further chemical modifications with various biomolecules. To our best knowledge, the NIR MnCuInS/ZnS@BSA nanoparticle and urchin-like Au nanoparticle are the first proposal as a donor-acceptor pair for enhanced FRET system.

Herein, an important biomarker-HER2 protein (human epidermal growth factor receptor 2, also called *c*-erbB2 or Neu), whose overexpression is associated with aggressive tumor growth, increased metastatic rates, poor clinical outcomes and significantly shortened disease-free and overall survival in patients with breast cancer [34,35], and whose detection in serum plays an important role in selecting appropriate therapy for patients, evaluating response during treatment, detecting recurrent metastatic breast cancer, and judging prognosis [36], was chosen as the target analyte by employing our novel donor-acceptor pair to construct a new and enhanced FRET biosensing platform (Scheme 1). The NIR-emitting MnCuInS/ZnS@BSA nanoparticles linked with HER2 aptamer (MnCuInS/ZnS@BSA-Apt) acted as fluorescence donors. The urchin-like Au NPs linked with the single stranded DNA (ssDNA) which is partially complementary to the HER2 aptamer (urchin-like Au NPs-ssDNA) acted as acceptors. Then FRET occurred by the binding between MnCuInS/ZnS@BSA-Apt and urchin-like Au NPs-ssDNA. When in the presence of HER2, FRET effect was broken, fluorescence increased. The combination of urchin-like Au NPs with NIR-emitting MnCuInS/ZnS@BSA nanocomposites had the advantage for the increase of FRET efficiency and could conveniently combined with other specific biological recognition events for a wide application in clinical diagnosis.

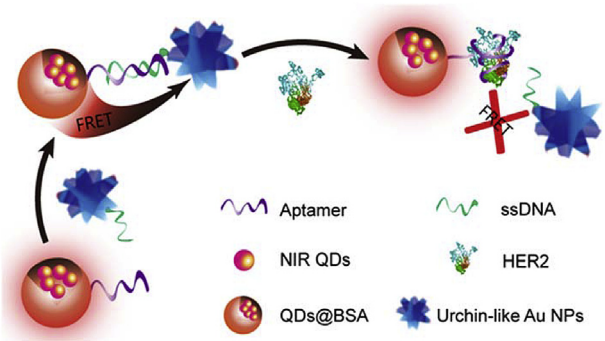

Scheme 1. Schematic illustration of the enhanced FRET system towards HER2 detection on the basis of NIR MnCuInS/ZnS@BSA and urchin-like Au NPs. Note that QDs@BSA is linked to the aptamer, and urchin-like Au NPs is linked to the ssDNA.

Please cite this article in press as: H. Xing, et al., Near-infrared MnCuInS/ZnS@BSA and urchin-like Au nanoparticle as a novel donor-acceptor pair for enhanced FRET biosensing, Analytica Chimica Acta (2018), https://doi.org/10.1016/j.aca.2018.05.048

2. Materials and methods

2.1. Reagents and materials

Manganese (II) acetate dehydrate (98%), copper (II) acetate (anhydrous, 98%), indium (III) acetate (99.99% metals basis), glutaraldehyde (25% aq. soln.), hydroquinone (99%) were purchased from Alfa Aesar Co., Ltd. 1-octadecene (ODE), gold (III) chloride trihydrate, *N*-hydroxysuccinimide (NHS; 98%), *N*-[3-(dimethylamino)propyl]-*N*′-ethylcarbodiimide (EDC), tris (2-carboxyethyl) phosphine hydrochloride (TCEP), and polyvinylpyrrolidone (PVP, powder, average Mw~55000) were purchased from Sigma-Aldrich Co., Ltd. Zinc acetate (99.99% metals basis), oleic acid (OA), oleylamine, 2-[morpholino]ethanesulfonic acid monohydrate (MES) were purchased from Aladdin Co., Ltd. Bovine serum albumin (BSA) was purchased from Shanghai Sangon Biological Engineering Technology and Services Co., Ltd. HER2 protein was purchased from Sino Biological Inc. Other chemicals were of analytical reagent grade. Ultrapure water obtained from a Milli-Q water purification system ($\geq$18 MΩ cm) was used in all measurements. The aptamer and the ssDNA were synthesized and purified by Takara Biomedical Technology Co., Ltd.

The sequences of the aptamer and ssDNA are as follows:Aptamer:5′-COOH-AAAAAAGCAGCGGTGTGGGGG-CAGCGGTGTGGGGGCAGCGGTGTGGGG-3′ssDNA:5′-SH-C6-AAAAAACCCCACACCGCT-3′

2.2. Instruments

Ultraviolet−visible (UV−vis) absorption spectra were carried out on a Cary 50 spectrophotometer (Varian, USA). The fluorescence spectra were obtained on a Fluoromax-4 spectrometer (Horiba, France). The transmission electron microscopy (TEM) images were obtained on a JEM-200CX instrument (Japan) using an accelerating voltage of 80 kV. The high-resolution transmission electron microscopy (HR-TEM) images were recorded on a JEOL-2100F apparatus at an accelerating voltage of 200 kV.

2.3. Synthesis of MnCuInS QDs

Alloyed MnCuInS quantum dots were prepared according to a literature with slight modification [37]. First, 0.1 mmol manganese (II) acetate, 0.05 mmol copper (II) acetate, 0.05 mmol indium (III) acetate, 5.0 mL of 1-octadecene and 0.2 mL of oleic acid were injected into a 50 mL three-neck flask. The mixture was degassed under vacuum for 15 min. Under argon flow, the reaction mixture was heated to 120 °C to form a blue clear solution. Then, 0.2 mL of 1-dodecanethiol was added into the reaction system. At the moment, the color of the solution changed from blue to pale yellow. Subsequently, 0.3 mmol sulfur dissolved in 1.0 mL of oleylamine was swiftly injected into the flask. Then the solution was heated to 140 °C and aged for 20 min.

2.4. In situ synthesis of MnCuInS/ZnS core/shell nanocrystals

The growth solution of MnCuInS QDs was cooled to 80 °C. Then 0.2 mmol zinc acetate dissolved in OA/ODE (the ratio of OA/ODE is 1/3, in total 1.0 mL) was added into the reaction solution. Next, the temperature of reaction solution was heated to 210 °C and kept at this temperature for 30 min to allow the growth of the ZnS. The reaction solution was cooled to room temperature. The product was obtained by centrifugation at 10000 rpm for 5 min and washed with cyclohexane for three times. Finally, MnCuInS/ZnS QDs were resuspended in cyclohexane and stored at room temperature shielded from light.

2.5. Formation of MnCuInS/ZnS@BSA

Briefly, 2.0 mL of BSA solution (5 mg mL^{-1}) was mixed with 160 μL of MnCuInS/ZnS QDs (10 mg mL^{-1}) and vigorous stirred at 300 rpm for 1 h. Then, the mixture was sonicated for 5 min. Subsequently, desolvation was performed with continuous and slowly addition of 7 mL anhydrous ethanol, and the solution was kept vigorous stirring at 700 rpm for 10 min. Next, 60 μL of 0.2% glutaraldehyde solution was injected into the suspension. The suspension was stirred for 16 h at room temperature to form stable MnCuInS/ZnS@BSA nanoparticles. The product was obtained by centrifugation at 10000 rpm for 10 min at 4 °C and rinsed with ultrapure water and ethanol three times. Finally, the obtained MnCuInS/ZnS@BSA nanoparticles were resuspended in phosphate buffered saline (PBS) buffer solution (10 mM, pH 7.4) and stored at 4 °C.

2.6. Synthesis of the urchin-like Au NPs

The preparation of Au seeds was performed as previously reported [38]. 75 μL of $HAuCl_4$ (100 mM) and 30 mL of ultrapure water were added to a flask. The mixture was heated to boiling. While boiling, 900 μL of sodium citrate aqueous solution (1 w/v %) was added to the flask quickly, then the solution was kept boiling for 10 min, until the color of the solution became wine red. The solution was cooled to obtain Au seeds. The urchin-like Au NPs was synthesized according to the reported method [38] with some modification. Briefly, 30 mM hydroquinone was foremost prepared by dissolving 33 mg hydroquinone into 10 mL of ultrapure water, which was used right after it was ready. 20 μL of $HAuCl_4$ (100 mM) was added to a flask containing 9.60 mL of ultrapure water. Subsequently, 25 μL of Au seeds, 22 μL of sodium citrate (1 w/v %) and 600 μL of hydroquinone (30 mM) were added and stirred at room temperature for 30 min. Then, in order to avoid the aggregation of the urchin-like Au NPs, 100 μL of PVP (10 mM in H_2O) was added into 1.0 mL of urchin-like Au NPs aqueous solution and stirred at room temperature for 30 min. At last, the urchin-like Au NPs were obtained by centrifugation at 8000 rpm for 5 min and washed twice. Then they were dispersed in 1.0 mL of PBS buffer for further usage.

2.7. Preparation of the MnCuInS/ZnS@BSA-Apt bioconjugates

The carboxyl-modified aptamer was covalently linked to MnCuInS/ZnS@BSA nanoparticles through the typical EDC/NHS protocol. First, to activate the COOH groups at aptamer, aptamer solution (4 μL, 100 μM) were added into 1.0 mL of MES buffer (0.1 M, 0.5 M NaCl, pH 6.0). 0.4 mg of EDC was then added. Almost immediately 0.6 mg of NHS was added to the reaction. The reaction components were mixed well for reaction for 15 min at room temperature. After that, Na_2HPO_4 solution (0.1 M, 2.0 mL) was added to increase the pH of solution above 7.0. Then, MnCuInS/ZnS@BSA solution (800 μL, 10 mg mL^{-1}) was added into the activated aptamer solution and stirred at 200 rpm for 4 h at room temperature. Finally, the reaction solution was centrifugation at 8000 rpm for 5 min and washed for three times to obtain MnCuInS/ZnS@BSA-Apt bioconjugates. At last, the MnCuInS/ZnS@BSA-Apt bioconjugates were resuspended in PBS buffer and stored at 4 °C.

2.8. Preparation of the Au-ssDNA bioconjugates

ssDNA solution (200 μM) dissolved in TE buffer (10 mM Tris-HCl, 1 mM EDTA, pH 8.0) was added to isopyknic 10 mM TCEP solution to react for 1 h at room temperature, and then 10 μL of the obtained 100 μM ssDNA solution was added into 1.0 mL of urchin-like Au NPs solution and stirred at 200 rpm for 2 h at room temperature

Please cite this article in press as: H. Xing, et al., Near-infrared MnCuInS/ZnS@BSA and urchin-like Au nanoparticle as a novel donor-acceptor pair for enhanced FRET biosensing, Analytica Chimica Acta (2018), https://doi.org/10.1016/j.aca.2018.05.048

shielded from light. After that, in order to block non-specific binding sites, 5 μL of 1% BSA in ultrapure water was added into the above reaction solution. Then, the reaction solution was stirred at 200 rpm in the dark for 0.5 h at room temperature. Finally, the Au-ssDNA was obtained by centrifugation at 2500 rpm for 3 min and dispersed in 10 mM PBS buffer (pH 7.4).

2.9. Construction of the enhanced FRET sensor for HER2 detection

In the process of HER2 sensing, 100 μL of MnCuInS/ZnS@BSA-Apt bioconjugates (10 mg mL^{-1}) and 100 μL of Au-ssDNA (5 mg mL^{-1}) were firstly mixed and incubated for 1 h at 37 °C. Afterwards, the mixture was diluted with PBS buffer and different amounts of HER2 protein were added into the mixture (total volume 300 μL). Finally, the mixture was incubated for another 1 h at 37 °C, and then the fluorescence spectra of the samples were recorded by fluorescence measurements.

3. Results and discussion

3.1. Characterization

NIR MnCuInS/ZnS QDs were firstly synthesized. A high-resolution transmission electron microscopy (HR-TEM) image clearly confirmed the successful preparation of MnCuInS/ZnS QDs, which exhibited approximately spherical in shape and good monodispersibility in cyclohexane (Fig. 1A and inset in Fig. 1D). The MnCuInS/ZnS QDs had a uniform size distribution and an average size of about 5 nm. Continuous lattice fringes was observed in HR-TEM image, indicating that the synthesized MnCuInS/ZnS QDs have high crystallinity. As shown in Fig. 1B, XRD data revealed that the crystal phase of MnCuInS/ZnS QD was mainly zincblende structure. Fig. 1C showed the UV–vis absorption spectrum of MnCuInS/ZnS QDs. The UV–vis spectrum showed wide-band absorption (from 300 to 800 nm) and exhibited absorption peak from 500 to 680 nm. Therefore, the fluorescence emission spectrum of MnCuInS/ZnS QDs was recorded from 630 to 800 nm at room temperature with a 600 nm excitation wavelength (Fig. 1D). The fluorescence emission spectrum displayed a maximum emission wavelength at 741 nm.

Next, MnCuInS/ZnS@BSA nanoparticles were prepared to enhance biocompatibility and water solubility according to the albumin desolvation method [39,40]. The formation process of MnCuInS/ZnS@BSA nanoparticles is illustrated in Fig. S1. BSA proteins were first incorporated with hydrophobic MnCuInS/ZnS QDs, and the specific hydrophobic sites of protein can bind with water-insoluble QDs. Then MnCuInS/ZnS@BSA nanoparticles were made by ethanol-induced albumin desolvation. Finally, glutaraldehyde was added to the suspension to form stable MnCuInS/ZnS@BSA nanoparticles. The size of MnCuInS/ZnS@BSA nanoparticles was determined by TEM. As shown in the TEM pattern (Fig. 2A), the MnCuInS/ZnS@BSA nanoparticles exhibited spherical morphology and the size of the MnCuInS/ZnS@BSA nanoparticles was estimated to be 100 nm. Compared with MnCuInS/ZnS QDs, the fluorescence emission spectrum of MnCuInS/ZnS@BSA nanoparticles had no significantly change, and also had a maximum emission wavelength at 741 nm (Fig. 2E).

To measure the efficiency of MnCuInS/ZnS QDs incorporation into BSA nanoparticles, 0.8 mg of MnCuInS/ZnS QDs was added into

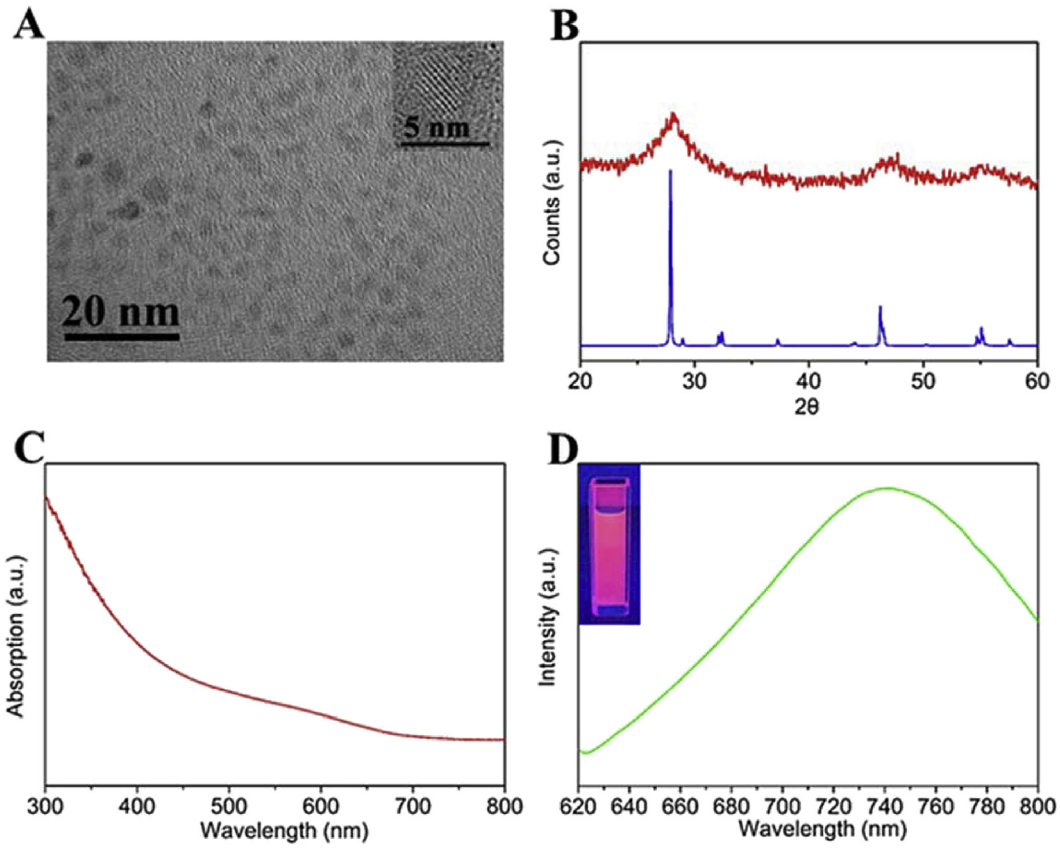

Fig. 1. (A) TEM image of MnCuInS/ZnS QDs. (B) XRD pattern of MnCuInS/ZnS QDs. (C) UV–vis absorption spectrum of MnCuInS/ZnS QDs. (D) Fluorescence emission spectrum of MnCuInS/ZnS QDs. Inset: (A) HR-TEM image of MnCuInS/ZnS QDs. (D) Photograph of MnCuInS/ZnS QDs solution in cyclohexane under UV light irradiation.

Please cite this article in press as: H. Xing, et al., Near-infrared MnCuInS/ZnS@BSA and urchin-like Au nanoparticle as a novel donor-acceptor pair for enhanced FRET biosensing, Analytica Chimica Acta (2018), https://doi.org/10.1016/j.aca.2018.05.048

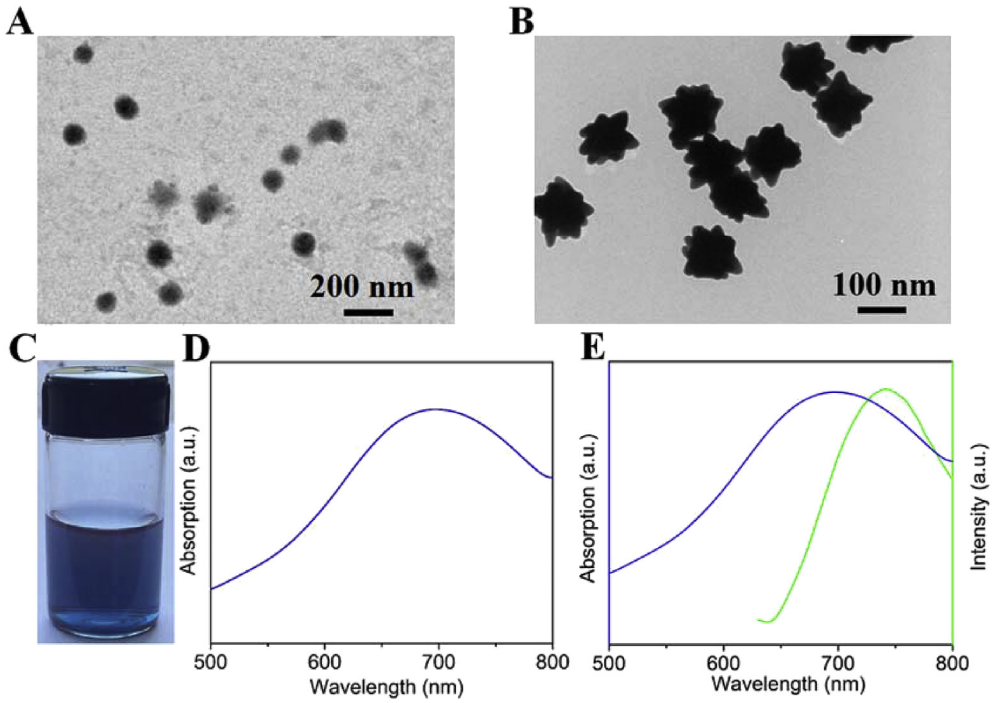

Fig. 2. (A) TEM image of MnCuInS/ZnS@BSA nanoparticles. (B) TEM image of urchin-like Au NPs. (C) Photograph of urchin-like Au NPs aqueous solution. (D) UV–vis absorption spectrum of urchin-like Au NPs. (E) UV–vis absorption spectrum of urchin-like Au NPs (left) and fluorescence emission spectrum of MnCuInS/ZnS@BSA nanoparticles (right).

the BSA solution. After the reaction, the supernatant was collected by centrifugation to separate unbound QDs from free BSA molecules. MnCuInS/ZnS QDs were quantified by measuring the fluorescence intensity at 741 nm. As shown in Fig. S2, the loading yield of MnCuInS/ZnS QDs in BSA nanoparticles was 94.13–95.5%, calculated with the following equation: loading yield (%) = (QDs used−unloaded QDs)/QDs used.

The toxicity of MnCuInS/ZnS@BSA nanoparticles was assessed by MTT assay, and the result was showed in Fig. S3. The cell viability was investigated with incubation with different concentrations of MnCuInS/ZnS@BSA nanoparticles. After incubating with MnCuInS/ZnS@BSA nanoparticles for 16 h, the absorbance had slight decrease and more than 90% of MCF-7 cells were still survive even at the concentration up to 13.32 mg mL^{-1} (the concentration of MnCuInS/ZnS@BSA nanoparticles used in this work was 3.33 mg mL^{-1}). This result shows that our QDs-based FRET system has hypotoxicity.

As to the fluorescence energy acceptor, the TEM image indicated that the prepared above Au NPs have an urchin morphology in shape with an average diameter of about 100 nm (Fig. 2B). The urchin-like Au NPs had favorable solubility in aqueous solution (Fig. 2C), which was conducive to homogeneous bioanalysis. As shown in Fig. 2D, the UV–vis absorption of urchin-like Au NPs showed a strong absorption band at 700 nm, ensuring good overlap with the fluorescence emission spectrum of MnCuInS/ZnS@BSA nanoparticles (Fig. 2E). Therefore, the FRET efficiency between MnCuInS/ZnS@BSA and urchin-like Au NPs was improved and the background signal of the biosensor was reduced.

In Fig. 3A, the UV–vis absorption of MnCuInS/ZnS@BSA-Apt had an obvious absorption band at 260 nm (curve a), which was the characteristic absorption band of aptamer. Meanwhile, the absorption spectrum of MnCuInS/ZnS@BSA nanoparticles showed no significant absorption from 220 to 350 nm, indicating the successful modification of aptamer to MnCuInS/ZnS@BSA nanoparticles. In addition, the successful conjugation between urchin-like Au NPs and ssDNA was also confirmed by UV–vis spectroscopy (Fig. 3B).

3.2. Characterization of the FRET system

The principle of the MnCuInS/ZnS@BSA-Au NPs FRET system is illustrated in Scheme 1. The HER2 aptamer was first attached to the surface of MnCuInS/ZnS@BSA nanoparticle to form MnCuInS/ZnS@BSA-Apt bioconjugate. The ssDNA which is partially complementary to the aptamer was bound with urchin-like Au NP to form Au-ssDNA. Then, MnCuInS/ZnS@BSA-Apt was effectively bound with Au NPs-ssDNA through the hybridization between the aptamer and the ssDNA, leading to a shortened distance between the donor and the acceptor. This phenomenon was confirmed in Fig. 3C, which shows the urchin-like Au NPs and MnCuInS/ZnS@BSA nanoparticles were bind together. Thus, FRET process from MnCuInS/ZnS@BSA to urchin-like Au NPs occurred naturally and the fluorescence of MnCuInS/ZnS@BSA was suppressed, and the sensor was turned off and had a low background signal. When the target-HER2 protein was added to the system, HER2 protein could bind to the aptamer and competed with the ssDNA, Au-ssDNA was separated from MnCuInS/ZnS@BSA-Apt (shown in Fig. 3D), resulting in fluorescence increase of MnCuInS/ZnS@BSA and the sensor was turned on. The above TEM characterization verified the feasibility of this MnCuInS/ZnS@BSA-Au NPs FRET system. Furthermore, since the MnCuInS/ZnS@BSA nanoparticles enhance NIR fluorescence emission, and the urchin-like Au NPs have strong NIR absorption, this donor-acceptor pair shows enhanced FRET phenomenon, thus improving overall performance of the assay.

3.3. HER2 sensing with the enhanced FRET system

Under the optimized conditions (Fig. S4), the fluorescence spectra responded to various concentrations of HER2 protein were further investigated. For this purpose, the biosensor was treated with different concentrations of HER2 protein and the fluorescence intensities were recorded. With the increase of the concentration of HER2 protein, the fluorescence emission

Please cite this article in press as: H. Xing, et al., Near-infrared MnCuInS/ZnS@BSA and urchin-like Au nanoparticle as a novel donor-acceptor pair for enhanced FRET biosensing, Analytica Chimica Acta (2018), https://doi.org/10.1016/j.aca.2018.05.048

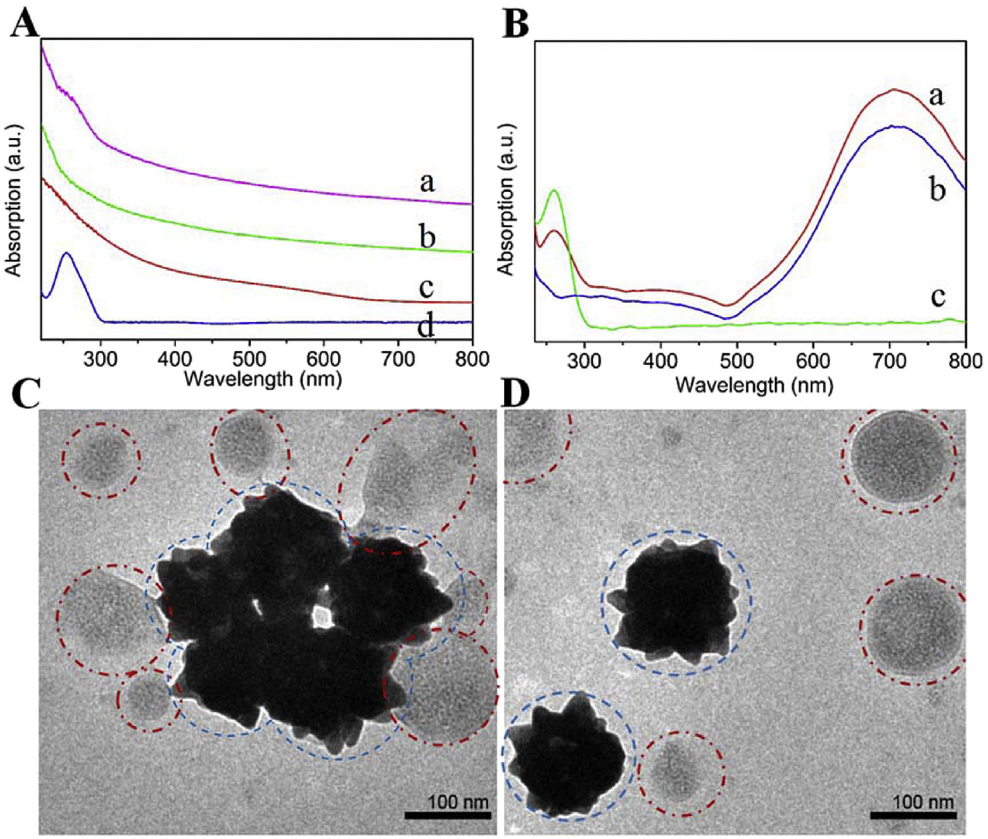

Fig. 3. (A) UV–vis absorption spectra of MnCuInS/ZnS@BSA-Apt (a), MnCuInS/ZnS@BSA (b), MnCuInS/ZnS (c), and aptamer (d). (B) UV–vis absorption spectra of urchin-like Au NPs-ssDNA (a), urchin-like Au NPs (b), ssDNA (c). Corresponding TEM images of the states of urchin-like Au NPs (blue dashed-line circle) and MnCuInS/ZnS@BSA nanoparticles (red dashed-line circle) before (C) and after (D) the HER2 protein added. (For interpretation of the references to color in this figure legend, the reader is referred to the Web version of this article.)

intensity of MnCuInS/ZnS@BSA was gradually increased as desired. This was due to the fact that the Au-ssDNA was replaced from the MnCuInS/ZnS@BSA-Apt surface by the HER2 protein. Therefore, the separation of the acceptor from the donor led to the fluorescence increase of MnCuInS/ZnS@BSA.

As shown in Fig. 4A, the fluorescence intensity of the biosensor increased with the increase of HER2 protein concentrations. In the absence of HER2 protein, the fluorescence intensity was lower than that in the presence of HER2 protein. More importantly, the fluorescence increase was positive correlated with the concentration of HER2 protein in the range from 2 to 100 ng mL^{-1} (Fig. 4B). The relative fluorescence intensity would deviate from the linear calibration curve when the concentration of HER2 protein was larger than 100 ng mL^{-1}. The linear calibration curve was constructed by plotting the relative fluorescence intensity ($(F\text{-}F_0)/F_0$) against lg C (C is the concentration of HER2 protein). The linear regression equation is $I = (F\text{-}F_0)/F_0 = -0.478 + 1.876 \lg C_{HER2}$. The linearity coefficient is 0.997 and the limit of detection of the HER2 protein is obtained to be 1 ng mL^{-1} at a signal-to-noise ratio of 3 (details of the determination of the detection limit are given in ESI). The linear range is wider and the detection limit is lower than most of the previously reported works (Table S1). In addition, the HER2 level in the serum of normal individuals is 2–15 ng mL^{-1}, whereas the breast cancer patients have elevated HER2 levels (15–75 ng mL^{-1}) [41–43]. Herein, the detection range and the limit of detection of the HER2 protein in our developed system has the ability to distinguish between people with the disease and healthy individuals.

3.4. Selectivity of the biosensor

In order to assess the specificity of this sensing system to HER2 protein, the responses of biosensor to other proteins including AFP, CEA, PSA and BSA was studied. As shown in Fig. 5A, only HER2 protein could cause significant fluorescence increase, while other protein molecules led to slight signal changes. In addition, as we know some metal ions can quench the QDs through cation exchange (ionic etching) [44], so the effects of different metal ions towards our FRET system were also investigated. As shown in Fig. 5B, metal ions did not lead significant signal changes and had almost no interference towards our FRET system. This may due to the BSA coating hindered the exposure of MnCuInS/ZnS QDs to metal ions, thus cation exchange was prevented. The above results indicated that the developed sensing strategy has good specificity for detecting HER2 protein.

3.5. Real sample detection of HER2 protein

The developed biosensor was employed to the detection of HER2 protein spiked in diluent serum samples for recovery test. Different concentrations of HER2 protein were directly added in 10-fold diluent normal human serum. The recoveries of HER2 protein were obtained in the range of 93.47–97.33% (Table S2). In addition, it was further applied to the detection of HER2 in three human serum samples: one collected from healthy patient and two collected from breast cancer patients. The results obtained with the biosensor were compared with those provided by a commercial ELISA kit (The calibration curve obtained by using the ELISA kit for

Please cite this article in press as: H. Xing, et al., Near-infrared MnCuInS/ZnS@BSA and urchin-like Au nanoparticle as a novel donor-acceptor pair for enhanced FRET biosensing, Analytica Chimica Acta (2018), https://doi.org/10.1016/j.aca.2018.05.048

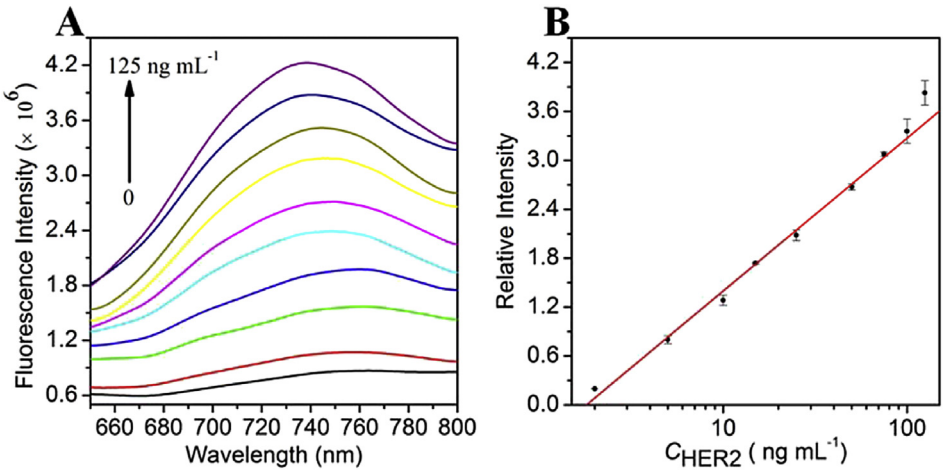

Fig. 4. (A) Fluorescence spectra toward various concentrations of HER2 protein (0, 2, 5, 10, 15, 25, 50, 75, 100, 125 ng mL^{-1}). (B) Linear relationship between fluorescence increase and the logarithm of the HER2 protein concentrations. Relative intensity ($(F-F_0)/F_0$), where F_0 represents the fluorescence intensity of the sensor in the blank solution, F is the intensity of the system added different concentrations of HER2 protein.

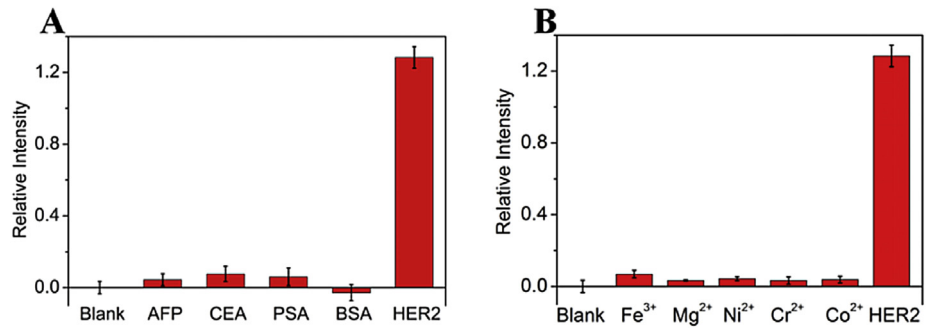

Fig. 5. Relative intensity ($(F-F_0)/F_0$) of the sensor toward (A) different interfering proteins, (B) different metal ions. The concentration of each added tested interfering protein was 20 ng mL^{-1} and each added tested interfering metal ions was 100 ng mL^{-1}. The concentration of HER2 protein was 10 ng mL^{-1}.

Table 1
HER2 determination by the fabricated HER2 FRET-based biosensor and ELISA method.

Samples	ELISA (ng mL^{-1})	FRET-biosensor (ng mL^{-1})
Breast cancer patient-1	95.02	90.81
	RSD $_{n=3}$ = 5.90 (%)	RSD $_{n=3}$ = 5.20 (%)
Breast cancer patient-2	55.86	55.22
	RSD $_{n=3}$ = 2.59 (%)	RSD $_{n=3}$ = 4.36 (%)
Healthy patient	14.86	14.49
	RSD $_{n=3}$ = 6.48 (%)	RSD $_{n=3}$ = 1.69 (%)

detection of HER2 protein was shown in Fig. S5). The results (Table 1) indicated that the reliability of this designed biosensor in real sample detection, and our developed system is a promising method for detection of HER2 protein in clinical applications.

4. Conclusions

In summary, we have developed a novel and enhanced FRET biosensing strategy by using the NIR MnCuInS/ZnS@BSA as the energy donor and the urchin-like Au NPs as the energy acceptor. Compared with traditional NIR QDs including CdTe, CdSe, CdS et al., MnCuInS/ZnS QDs had lower toxicity. Meanwhile, we further encapsulated the NIR MnCuInS/ZnS QDs into BSA nanoparticles to amplify the fluorescence emission and enable their water-soluble stability. In addition, compared with the ordinary Au NPs, the urchin-like Au NPs had several advantages including novel structure, tunable diameter, strong NIR absorption, and good solubility. With the MnCuInS/ZnS@BSA and urchin-like Au NPs as a novel donor-acceptor pair, the enhanced FRET assay showed high sensitivity, good specificity and high precision in detection of HER2 protein. Furthermore, as different aptamers could specifically bind to different target proteins, this enhanced FRET biosensing platform can conveniently combine with other specific biological recognition events for a wider application in clinical diagnosis.

Acknowledgement

This work was supported by the Natural Science Foundation of China (No. 21625502, No. 21475062 and No. 21705079), the Natural Science Foundation of Jiangsu Province (BK20171033), and the Natural Science Foundation of the Jiangsu Higher Education Institutions of China (17KJB150026). We appreciate the financial support from the Priority Academic Program Development of Jiangsu Higher Education Institutions and the Program for Jiangsu Collaborative Innovation Center of Biomedical Functional Materials.

Appendix A. Supplementary data

Supplementary data related to this article can be found at https://doi.org/10.1016/j.aca.2018.05.048.

Please cite this article in press as: H. Xing, et al., Near-infrared MnCuInS/ZnS@BSA and urchin-like Au nanoparticle as a novel donor-acceptor pair for enhanced FRET biosensing, Analytica Chimica Acta (2018), https://doi.org/10.1016/j.aca.2018.05.048

References

[1] Y. Wang, D. Gao, P. Zhang, P. Gong, C. Chen, G. Gao, L. Cai, A near infrared fluorescence resonance energy transfer based aptamer biosensor for insulin detection in human plasma, Chem. Commun 50 (2014) 811–813.
[2] Y. Wang, K. Jiang, J. Zhu, L. Zhang, H. Lin, A FRET-based carbon dot-MnO_2 nanosheet architecture for glutathione sensing in human whole blood samples, Chem. Commun 51 (2015) 12748–12751.
[3] Y. Yang, J. Huang, X. Yang, K. Quan, H. Wang, L. Ying, N. Xie, M. Ou, K. Wang, FRET nanoflares for intracellular mRNA detection: avoiding false positive signals and minimizing effects of system fluctuations, J. Am. Chem. Soc. 137 (2015) 8340–8343.
[4] N. Aissaoui, K. Moth-Poulsen, M. Kall, P. Johansson, L.M. Wilhelmsson, B. Albinsson, FRET enhancement close to gold nanoparticles positioned in DNA origami constructs, Nanoscale 9 (2017) 673–683.
[5] X.L. Li, N. Hao, H.Y. Chen, J.J. Xu, Tumor-marker-mediated "on-demand" drug release and real-time monitoring system based on multifunctional mesoporous silica nanoparticles, Anal. Chem. 86 (2014) 10239–10245.
[6] L. Li, J. Liu, X. Yang, Z. Peng, W. Liu, J. Xu, J. Tang, X. He, K. Wang, Quantum dot/methylene blue FRET mediated NIR fluorescent nanomicelles with large Stokes shift for bioimaging, Chem. Commun 51 (2015) 14357–14360.
[7] Y.R. Li, Q. Liu, Z. Hong, H.F. Wang, Magnetic separation-assistant fluorescence resonance energy transfer inhibition for highly sensitive probing of nucleolin, Anal. Chem. 87 (2015) 12183–12189.
[8] X. Qiu, N. Hildebrandt, Rapid and multiplexed microRNA diagnostic assay using quantum dot-based förster resonance energy transfer, ACS Nano 9 (2015) 8449–8457.
[9] A. Shahmuradyan, U.J. Krull, Intrinsically labeled fluorescent oligonucleotide probes on quantum dots for transduction of nucleic acid hybridization, Anal. Chem. 88 (2016) 3186–3193.
[10] X. Huang, Y. Liu, B. Yung, Y. Xiong, X. Chen, Nanotechnology-enhanced no-wash biosensors for in vitro diagnostics of cancer, ACS Nano 11 (2017) 5238–5292.
[11] Y. Wang, X. Liu, J. Zhang, D. Aili, B. Liedberg, Time-resolved botulinum neurotoxin A activity monitored using peptide-functionalized Au nanoparticle energy transfer sensors, Chem. Sci. 5 (2014) 2651–2656.
[12] L.J. Wang, Y. Yang, C.Y. Zhang, Phosphorylation-directed assembly of a single quantum dot based nanosensor for protein kinase assay, Anal. Chem. 87 (2015) 4696–4703.
[13] Y. Liang, X. Huang, R. Yu, Y. Zhou, Y. Xiong, Fluorescence ELISA for sensitive detection of ochratoxin A based on glucose oxidase-mediated fluorescence quenching of CdTe QDs, Anal. Chim. Acta 936 (2016) 195–201.
[14] H. Pan, P. Zhang, D. Gao, Y. Zhang, P. Li, L. Liu, C. Wang, H. Wang, Y. Ma, L. Cai, Noninvasive visualization of respiratory viral infection using bioorthogonal conjugated near infrared-emitting quantum dots, ACS Nano 8 (2014) 5468–5477.
[15] M. Yu, K. Zhao, X. Zhu, S. Tang, Z. Nie, Y. Huang, P. Zhao, S. Yao, Development of near-infrared ratiometric fluorescent probe based on cationic conjugated polymer and CdTe/CdS QDs for label-free determination of glucose in human body fluids, Biosens. Bioelectron. 95 (2017) 41–47.
[16] J. Wang, H. Han, X. Jiang, L. Huang, L. Chen, N. Li, Quantum dot-based near-infrared electrochemiluminescent immunosensor with gold nanoparticle-graphene nanosheet hybrids and silica nanospheres double-assisted signal amplification, Anal. Chem. 84 (2012) 4893–4899.
[17] P.J. Wu, S.Y. Kuo, Y.C. Huang, C.P. Chen, Y.H. Chan, Polydiacetylene-enclosed near-infrared fluorescent semiconducting polymer dots for bioimaging and sensing, Anal. Chem. 86 (2014) 4831–4839.
[18] A.B. Chinen, C.M. Guan, J.R. Ferrer, S.N. Barnaby, T.J. Merkel, C.A. Mirkin, Nanoparticle probes for the detection of cancer biomarkers, cells, and tissues by fluorescence, Chem. Rev. 115 (2015) 10530–10574.
[19] E. Oh, M.Y. Hong, D. Lee, S.H. Nam, H.C. Yoon, H.S. Kim, Inhibition assay of biomolecules based on fluorescence resonance energy transfer (FRET) between quantum dots and gold nanoparticles, J. Am. Chem. Soc. 127 (2005) 3270–3271.
[20] K.E. Sapsford, L. Berti, I.L. Medintz, Materials for fluorescence resonance energy transfer analysis: beyond traditional donor-acceptor combinations, Angew. Chem. Int. Ed. 45 (2006) 4562–4589.
[21] J. Shi, C. Chan, Y. Pang, W. Ye, F. Tian, J. Lyu, Y. Zhang, M. Yang, A fluorescence resonance energy transfer (FRET) biosensor based on graphene quantum dots (GQDs) and gold nanoparticles (AuNPs) for the detection of mecA gene sequence of Staphylococcus aureus, Biosens. Bioelectron. 67 (2015) 595–600.
[22] K. Shao, B. Wang, S. Ye, Y. Zuo, L. Wu, Q. Li, Z. Lu, X. Tan, H. Han, Signal-amplified near-infrared ratiometric electrochemiluminescence aptasensor based on multiple quenching and enhancement effect of graphene/gold nanorods/G-quadruplex, Anal. Chem. 88 (2016) 8179–8187.
[23] P. Zhao, K. He, Y. Han, Z. Zhang, M. Yu, H. Wang, Y. Huang, Z. Nie, S. Yao, Near-infrared dual-emission quantum dots-gold nanoclusters nanohybrid via co-template synthesis for ratiometric fluorescent detection and bioimaging of ascorbic acid in vitro and in vivo, Anal. Chem. 87 (2015) 9998–10005.
[24] H. Sun, H. Zhang, J. Ju, J. Zhang, G. Qian, C. Wang, B. Yang, Z.Y. Wang, One-step synthesis of high-quality gradient CdHgTe nanocrystals: a prerequisite to prepare CdHgTe-polymer bulk composites with intense near-infrared photoluminescence, Chem. Mater. 20 (2008) 6764–6769.
[25] G.X. Liang, L.L. Li, H.Y. Liu, J.R. Zhang, C. Burda, J.J. Zhu, Fabrication of near-infrared-emitting CdSeTe/ZnS core/shell quantum dots and their electro-generated chemiluminescence, Chem. Commun 46 (2010) 2974–2976.
[26] L.N. Chen, J. Wang, W.T. Li, H.Y. Han, Aqueous one-pot synthesis of bright and ultrasmall CdTe/CdS near-infrared-emitting quantum dots and their application for tumor targeting in vivo, Chem. Commun 48 (2012) 4971–4973.
[27] L. Mattera, S. Bhuckory, K.D. Wegner, X. Qiu, F. Agnese, C. Lincheneau, T. Senden, D. Djurado, L.J. Charbonniere, N. Hildebrandt, P. Reiss, Compact quantum dot-antibody conjugates for FRET immunoassays with sub-nanomolar detection limits, Nanoscale 8 (2016) 11275–11283.
[28] H. Nakamura, W. Kato, M. Uehara, K. Nose, T. Omata, S. Otsuka-Yao-Matsuo, M. Miyazaki, H. Maeda, Tunable photoluminescence wavelength of chalcopyrite $CuInS_2$-based semiconductor nanocrystals synthesized in a colloidal system, Chem. Mater. 18 (2006) 3330–3335.
[29] R.G. Xie, M. Rutherford, X.G. Peng, Formation of high-quality I-III-VI semiconductor nanocrystals by tuning relative reactivity of cationic precursors, J. Am. Chem. Soc. 131 (2009) 5691–5697.
[30] L. Chang, X. He, L. Chen, Y. Zhang, A novel fluorescent turn-on biosensor based on QDs@GSH-GO fluorescence resonance energy transfer for sensitive glutathione S-transferase sensing and cellular imaging, Nanoscale 9 (2017) 3881–3888.
[31] P. Wu, X.P. Yan, Doped quantum dots for chemo/biosensing and bioimaging, Chem. Soc. Rev. 42 (2013) 5489–5521.
[32] J. Zhou, Y. Yang, C.Y. Zhang, Toward biocompatible semiconductor quantum dots: from biosynthesis and bioconjugation to biomedical application, Chem. Rev. 115 (2015) 11669–11717.
[33] M. Michalska, A. Florczak, H. Dams-Kozlowska, J. Gapinski, S. Jurga, R. Schneider, Peptide-functionalized ZCIS QDs as fluorescent nanoprobe for targeted HER2-positive breast cancer cells imaging, Acta Biomater. 35 (2016) 293–304.
[34] T.Y. Rakovich, O.K. Mahfoud, B.M. Mohamed, A. Prina-Mello, K. Crosbie-Staunton, T. Van den Broeck, L. De Kimpe, A. Sukhanova, D. Baty, A. Rakovich, S.A. Maier, F. Alves, F. Nauwelaers, I. Nabiev, P. Chames, Y. Volkov, Highly sensitive single domain antibody-quantum dot conjugates for detection of HER2 biomarker in lung and breast cancer cells, ACS Nano 8 (2014) 5682–5695.
[35] U. Eletxigerra, J. Martinez-Perdiguero, R. Barderas, J.M. Pingarron, S. Campuzano, S. Merino, Surface plasmon resonance immunosensor for ErbB2 breast cancer biomarker determination in human serum and raw cancer cell lysates, Anal. Chim. Acta 905 (2016) 156–162.
[36] W.P. Carney, R. Neumann, A. Lipton, K. Leitzel, S. Ali, C.P. Price, Monitoring the circulating levels of the HER2/neu oncoprotein in breast cancer, Clin. Breast Canc. 2 (2004) 105–116.
[37] Q. Liu, R. Deng, X. Ji, D. Pan, Alloyed Mn-Cu-In-S nanocrystals: a new type of diluted magnetic semiconductor quantum dots, Nanotechnology 23 (2012) 255706.
[38] J. Li, J. Wu, X. Zhang, Y. Liu, D. Zhou, H. Sun, H. Zhang, B. Yang, Controllable synthesis of stable urchin-like gold nanoparticles using hydroquinone to tune the reactivity of gold chloride, J. Phys. Chem. C 115 (2011) 3630–3637.
[39] T. Wei, D. Du, Z. Wang, W. Zhang, Y. Lin, Z. Dai, Rapid and sensitive detection of microRNA via the capture of fluorescent dyes-loaded albumin nanoparticles around functionalized magnetic beads, Biosens. Bioelectron. 94 (2017) 56–62.
[40] Z. Wang, J. Li, J. Cho, A.B. Malik, Prevention of vascular inflammation by nanoparticle targeting of adherent neutrophils, Nat. Nanotechnol. 9 (2014) 204–210.
[41] A. Tabasi, A. Noorbakhsh, E. Sharifi, Reduced graphene oxide-chitosan-aptamer interface as new platform for ultrasensitive detection of human epidermal growth factor receptor 2, Biosens. Bioelectron. 95 (2017) 117–123.
[42] A. Qureshi, Y. Gurbuz, J.H. Niazi, Label-free capacitance based aptasensor platform for the detection of HER2/ErbB2 cancer biomarker in serum, Sensor. Actuator. B Chem. 220 (2015) 1145–1151.
[43] H. Ilkhani, A. Ravalli, G. Marrazza, Design of an affibody-based recognition strategy for human epidermal growth factor receptor 2 (HER2) detection by electrochemical biosensors, Chemosensors 4 (2016) 23.
[44] X.Y. Liu, G.B. Braun, M.D. Qin, E. Ruoslahti, K.N. Sugahara, In vivo cation exchange in quantum dots for tumor-specific imaging, Nat. Commun. 8 (2017) 343.

Please cite this article in press as: H. Xing, et al., Near-infrared MnCuInS/ZnS@BSA and urchin-like Au nanoparticle as a novel donor-acceptor pair for enhanced FRET biosensing, Analytica Chimica Acta (2018), https://doi.org/10.1016/j.aca.2018.05.048